Chapter 2
Computational Discovery of New High-Nitrogen Energetic Materials

Brad A. Steele and Ivan I. Oleynik

Abstract High-nitrogen-content energetic compounds containing multiple N–N bonds are an attractive candidate for new generation of environmentally friendly, and more powerful energetic materials. High-N content translates into much higher heat of formation resulting in much larger energy output, detonation pressure, and velocity upon conversion to large amounts of non-toxic, strongly bonded N_2 gas. This chapter describes recent advances in the computational discovery of a new family of polynitrogen pentazolate compounds using powerful first-principles evolutionary crystal structure prediction methods. After description of the methodology of the first-principles crystal structure prediction, several new high-nitrogen-content energetic compounds are described. In addition to providing information on structure and chemical composition, theory/simulations also suggests specific precursors, and experimental conditions that are required for experimental synthesis of such high-N pentazolate energetic materials. To aid in experimental detection of newly synthesized compounds, XRD patterns and corresponding Raman spectra are calculated for several candidate structures. The ultimate success was achieved in joint theoretical and experimental discovery of cesium pentazolate, which was synthesized by compressing and heating cesium azide CsN_3 and N_2 precursors in diamond anvil cell. This success story highlights the key role of first-principles structure prediction simulations in guiding experimental exploration of new high-N energetic materials.

2.1 Introduction

Energetic materials (EMs) are condensed phase compounds that are used as explosives, propellants and pyrotechnics [1]. Although their development can be traced back to ancient times, commercial large-scale production of EMs began only in nineteenth century when Alfred Nobel introduced nitroglycerin-based explosive

B. A. Steele · I. I. Oleynik (✉)
Department of Physics, University of South Florida, 4202 E. Fowler Ave, Tampa, FL 33620, USA
e-mail: oleynik@usf.edu

N. Goldman (ed.), *Computational Approaches for Chemistry Under Extreme Conditions*, Challenges and Advances in Computational Chemistry and Physics 28,
https://doi.org/10.1007/978-3-030-05600-1_2

Dynamite in 1867 [2]. Since then, several more powerful EMs were developed at the end of nineteenth and in twentieth centuries that are currently used in munitions, rocket propulsion, mining, construction, and demolition [1]. These EMs are molecular crystals such as trinitrotoluene (TNT), pentaerythritol tetranitrate (PETN), cyclotrimethylenetrinitramine (RDX), cyclotetramethylene tetranitramine (HMX), and triaminotrinitrobenzene (TATB) [1]. They consist of organic C–H–N–O molecules, which combine both fuel (C–H backbone) and oxidizer (nitro (NO_2) or nitrate (NO_3) groups within a single molecule. Upon initiation by impact or heating, such compounds react violently and release energy due to exothermic conversion of the constituent molecules in condensed phase to gas phase products such as CO/CO_2, H_2O, N_2 and solid carbon. The amount of energy released depends on the effectiveness of the C–H oxidation by NO_2 and NO_3 and the amount of nitrogen in constituent molecules. In particular, the conversion of nitrogen to very strong triply bonded N_2 results in an enormous release of energy. These factors are quantified by the notions of oxygen balance and nitrogen content.

Development of traditional C–H–N–O energetic materials faces a stumbling block as their poor oxygen balance and low nitrogen content cannot be further improved [1]. Moreover, their high initiation sensitivity resulting to accidental explosions and their toxicity are of great concern. High-nitrogen-content (high-N) energetic compounds with multiple N–N bonds are attractive alternative towards developing new generation of environmentally friendly, and more powerful EMs. High-N content translates into much higher heat of formation resulting in much larger energy output, detonation pressure and velocity upon conversion to large amounts of non-toxic, strongly bonded N_2 gas.

Compared to carbon, nitrogen is a unique element: N–N double bond is more than twice strong as single N–N bond and triple bond—more than three times strong as single N–N bond, which is not the case for the C–C bonds. As a result, carbon prefers to form extended compounds with mostly single C–C bonds, whereas nitrogen prefers to be in molecular triply bonded N≡N form. Due to this energetic preference, most of double- and single-bonded high-nitrogen compounds, if they exist, should be metastable at ambient pressure and temperature, i.e., their structure is locked in one of the energy minima separated from N≡N global minimum by an appreciable energy barrier. Application of high pressure and temperature (high-P-T) facilitates the efficient synthesis of such high-N compounds, by providing additional stimuli for breaking the strong intramolecular bonds of the original molecular precursors and forming new N–N bonds of the high-N products.

These single- and double-bonded metastable forms of pure nitrogen, if synthesized, are ultimate energetic materials as their conversion to N_2 would result in up to ten times increase in detonation pressure [3]. In 1992 Mailhiot et al. predicted the existence of such single-bonded pure nitrogen cubic gauche (cg-N) crystal structure and showed it is thermodynamically stable over N_2 molecular solid above 50 GPa [4]. Motivated by this theoretical prediction, in 2004 Eremets et al. successfully synthesized the cg-N at 110 GPa and 2,000 K [5]. Unfortunately, the cubic cg-N phase of nitrogen reverts to the molecular form around 40 GPa [6]. Subsequent attempts to recover cg-N at ambient conditions were unsuccessful [6–8].

One of the alternative routes towards synthesis of metastable poly-nitrogen EMs includes stabilization of single and double N–N bonding via addition of small amounts of atoms of other elements into pure nitrogen subsystem to cause the redistribution of electrons in the system resulting in change in character of chemical bonding. The competition between ionic and covalent bonding might promote new nitrogen phases other than triply bonded N_2. Then, the fundamental questions are whether such addition would result in stabilization of novel forms of single and double-bonded nitrogen in condensed phase, what is the role of pressure in overcoming energy barriers associated with such transformations, and what are the suitable precursors and optimal conditions for their synthesis?

To answer these questions, an extensive exploration of bonding and structure is required as a function of pressure, temperature, and chemical composition. A purely experimental approach would be extremely time-consuming and less certain as there are many unknowns at the molecular and atom-scale levels that cannot be uncovered due to limitation of experimental capabilities. Although theory/simulation does have its own limitations, in most cases it can answer the questions that are difficult or even impossible to address using experimental techniques especially those dealing with the atomic scale. Therefore, computational exploration of novel high-N compounds is an attractive alternative that allows for systematic investigation of these new compounds at the atomic scale. The ultimate goal of theory/modeling is to guide experiment by predicting composition-structure phase diagrams of novel high-N compounds, characterize the most energetically preferred materials and suggest specific synthesis routes towards realization of high-PT synthesis. However, to be successful in this formidable endeavor efficient methods for crystal structure prediction are required to make meaningful predictions.

This chapter describes recent advances that were made recently in computational discovery of a new family of polynitrogen alkali and hydronitrogen pentazolate compounds, all of them containing pentazolate N_5^- anion, the last all-nitrogen member of the azole series. Such discovery was made possible through application of powerful first-principles evolutionary crystal structure prediction methods. Importantly, theory/simulations also suggested specific precursors, and experimental conditions that are required for experimental synthesis of high-N pentazolate EMs. To aid in experimental detection of newly synthesized compounds, XRD patterns and corresponding Raman spectra were calculated for several candidate structures. The ultimate success was achieved in joint theoretical and experimental discovery of cesium pentazolate, which was synthesized by compressing and heating cesium azide CsN_3 and N_2 precursors in diamond anvil cell. This success story highlights the key role of first-principles structure prediction simulations in guiding experimental exploration of new high-N energetic materials.

2.2 First-Principles Crystal Structure Prediction

The crystal structure prediction problem is formulated as follows: given a set of specific chemical elements, determine all stable crystal phases and stoichiometries of all chemically stable compounds consisting of these elemental species at specified pressure and temperature. Mathematically, such a problem involves determination of the local and global minima as a function of atomic coordinates of multi-dimensional free energy surface. The solution of this problem is being considered as a grand challenge of theoretical materials chemistry [9]. The brute-force approach to crystal structure prediction would involve generation of all possible atomic arrangements in all possible crystals, optimization of geometrical parameters to get the free energy for each structure, and then determination of the structure at the lowest energy minimum. It is possible to show that the computational expense of such calculation scales exponentially with the number of atoms in the system. For example, finding the energy minimum of the system consisting of 10 atoms would involve 10^{11} combinations of different arrangements of the atoms, which will require the total computational time $\sim 10^3$ years, thus making this approach impractical [10].

In spite of the enormous complexity of the problem, there are several key features of the energy landscape of a complex system of atoms arranged in the crystal structure that make theoretical structure prediction possible [11, 12]. The simplification of the structure search problem occurs when each crystal is optimized, i.e., brought to a local minimum. Such optimization introduces chemical constraints on bond lengths, bond angles, resulting in avoidance of unfavorable contacts between atoms and overall reduction of dimensionality of the potential energy surface.

Another important feature simplifying the global energy landscape is clustering of several structures into basins of attraction (i.e., the same energy minimum) upon their geometry optimization [11]. The basins are typically arranged such that if one hops from one basin to another one, it is more likely the neighboring basin will have a lower energy and the energy barrier between them is small. It turned out that the low-energy basins tend to occur near each other, although they can be widely separated in clumps of low-energy basins. These basics facts tremendously simplify the complexity, thus making the crystal structure prediction possible.

There are several popular state-of-the-art structure prediction codes including random structure searching AIRSS [11], particle swamp optimization code CALYPSO [13] and universal structure predictor method USPEX [10]. The research on computational prediction of high-N EMs reviewed in this chapter has been performed using USPEX, which covers basic functionalities of the first two search methods, AIRSS and CALYPSO. The efficiency of USPEX is based on its carefully designed set of variation operators that allow to produce increasingly lower energy structures in subsequent generations. The USPEX method has been successfully applied to predict several novel crystal structures at high pressures that have been confirmed by experiment such as layered polymeric nitrogen [14, 15], a sodium chloride compound with unexpected Na_3Cl stoichiometry [16], superconducting H_3S [17, 18], and an ionic form of boron [19], to mention a few.

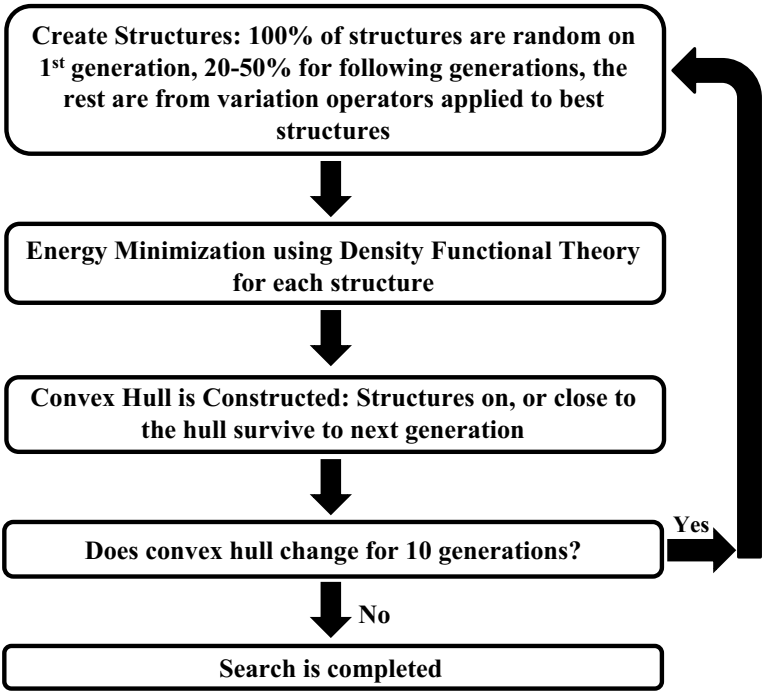

Fig. 2.1 Calculation flow diagram of the crystal structure prediction method USPEX

In the USPEX method, the structure search algorithm deals with generations—a set of crystal structures (individuals), that evolve from generation to generation. The overall schematic of the crystal structure search as implemented in USPEX code is given in Fig. 2.1. The search begins by creating the first generation consisting of random crystal structures with random atomic positions and lattice parameters, followed by the structure optimization of each individual from the first generation. This involves optimization of the atomic positions and lattice parameters at a given pressure of each individual to achieve the minimum of its total enthalpy at a given pressure. The total energy and enthalpy are calculated using first-principles density functional theory.

The computational time is saved by imposing distance constraints that prevent the atoms from being nonphysically close to each other. Constraints are also imposed on the minimum length of all the lattice parameters to prevent them from being too small. In addition, an initial guess for the volume is made based on values of the atomic volumes at a given pressure. The population size, i.e., a fixed number of individuals in each generation, is an important parameter, which is chosen to ensure structural and chemical diversity in each generation. Otherwise, the structure search will get trapped. The number and chemical nature of the atoms in each generated crystal are randomly sampled within a specified range as well as a given set of specific elements.

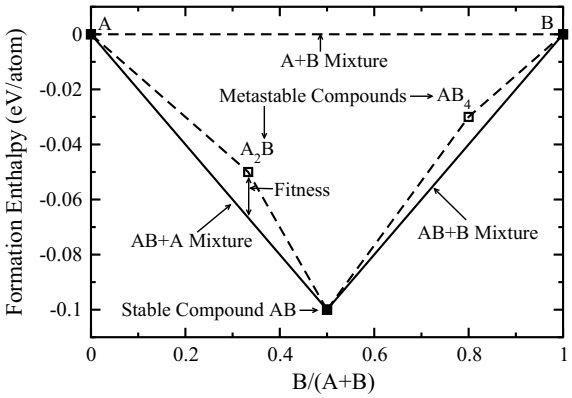

Fig. 2.2 Schematic of a convex hull for a binary system that consists of elements A and B. There are two metastable compounds A_2B and AB_4, their fitness being defined by the vertical distance from the convex hull. Both A_2B and AB_4 are thermodynamically unstable as they may decompose into a mixture of AB+A and AB+B compounds respectively

The complexity, which is defined as a total number of possible structures in a fixed volume, increases rapidly with the number of atoms. This is why using more atoms in the unit cell requires much larger population size.

USPEX can be used to search for binary (A_xB_y), ternary ($A_xB_yC_z$), and higher compositional dimensionality structures, by varying the number of atoms of type A, B, C, … in the unit cell. In the case of a binary search A_xB_y with the number of atoms restricted to be within the range of $\sim 8-20$ atoms per unit cell, a combinatorial calculation gives the estimate for the total number of possible chemical compositions ~ 150. Typical structure search involves about two to three structures per composition on the first generation (random structures only in the first generation and about one random structure per composition in each subsequent generation). By including additional random structures in each generation, trapping in one of the local potential energy minima is avoided.

The algorithm of structure search at a given pressure requires construction of the so-called convex hull for each generation. The convex hull is the convex envelope in the stoichiometry-formation enthalpy space, which is constructed by plotting data points corresponding to each optimized individual of the generation, see Fig. 2.2. In the case of a binary search A_xB_y, the lowest enthalpy data points are connected by line segments, starting from the pure elemental structure A all the way to B, avoiding the stoichiometries that would violate the convex nature of this envelope, see Fig. 2.2.

The formation enthalpy of A_xB_y compound is defined as $H_f(A_xB_y) = \big(H(A_xB_y) - xH(A) - yH(B)\big)/(x+y)$, where H() is the enthalpy of the corresponding material. The convex hull represents the set of *thermodynamically* stable compounds (A_xB_y) at a given pressure and temperature, Fig. 2.2. Lines connecting each pair of binary compounds represent the mixture of the two compounds: the formation enthalpy of each mixture represented by a point on a line is calculated using formation enthalpies of constituent compounds assuming that the interaction energy between two phases is negligible. If a compound is represented by a data point above the convex hull line, then it is thermodynamically unstable and will decompose into the two compounds at the ends of the corresponding line segment of the convex

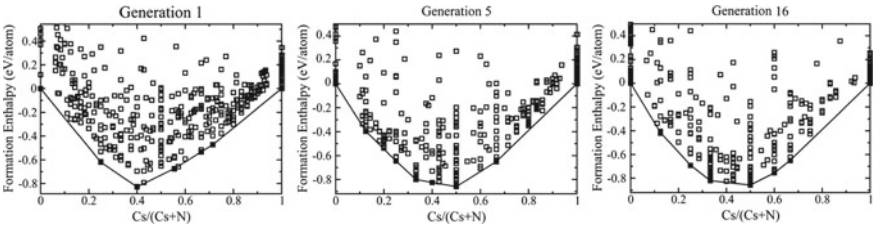

Fig. 2.3 Typical evolution of the calculated convex hull from the first generation to the last generation. The filled squares represent stable compounds on the convex hull. They change from generation to generation until the convex hull is converged

hull. For example, thermodynamically unstable compounds A_2B and AB_4 in Fig. 2.2 may decompose into a mixture of AB+A and AB+B compounds respectively. The compounds represented by the vertices of the convex hull constitute the full set of thermodynamically stable compounds at a given pressure.

To build the next generation, the structures in the previous generation are optimized by DFT and then ranked based on their fitness, which is referred to as the distance from the convex hull line (for binary systems) or from the convex plane (for ternary systems). The fittness is the major descriptor of the evolutionary crystal structure search. In the case of a single element compound, the structures are ranked by their enthalpy per atom (from the lowest to the highest). Then, a fraction of the best structures (typically 60%) from previous generation is selected and variation operators are applied to produce a subset of structures for a new generation. The kind of variation operators varies but it usually involves displacing the atoms and changing lattice parameters by a random value, merging two structures together, swapping atoms, transmutation of atoms into other atoms, etc. In addition, a prescribed fraction (typically 20–50%) of randomly generated structures are also added to every generation. Once the new generation is created, the search cycle is repeated by optimizing every individual of the new generation, constructing the convex hull, ranking individuals and building a new generation, see Fig. 2.1.

A typical evolution of the convex hull from the first generation to the last is shown in Fig. 2.3. With each generations new structures and stoichiometries may appear on the hull. The structures with stoichiometries that lie closer to the hull (a small fitness value) are given higher priority in the evolutionary algorithm designed by USPEX and variation operators are applied to them more often. One desirable feature that can bee seen in Fig. 2.3 is that the first generation is not dramatically different than the last generation, which implies that the first generation has enough individuals to produce a diverse and somewhat high-quality hull. In fact some of the compounds on the hull in the first generation are still on the hull in the final generation, see Fig. 2.3.

The structure search stops under assumption that the entire energy landscape is covered. In practice, it runs until it does not produce any new structures for several generations. Then, it is advisable to rerun the search again with differently generated random structures in the first generation, to make sure that the same structures are

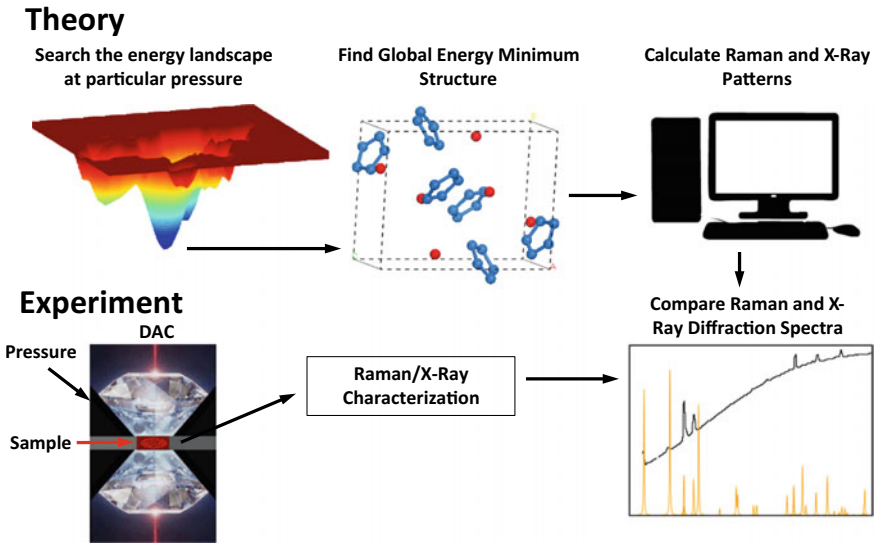

Fig. 2.4 Schematic of combined experimental and theoretical approaches for materials discovery at high pressures. The theoretical thrust involves searching the energy landscape, identifying new crystalline materials as the minima of the multi-dimensional potential energy surface, and calculating corresponding XRD patterns and Raman spectra. Experimental thrust includes compressing and heating the material in a diamond anvil cell (DAC), followed by characterizing the reaction products using Raman spectra and X-Ray diffraction patterns. The two methods come together when comparing the calculated and experimental spectra

found. An additional validation of the search involves predicting a crystal that is already known to exist from experiment: if the structure search finds this structure without any experimental input then the search may be considered to be performed adequately. Care must be taken when the experimental structure is complex (i.e. consists of a large number of atoms), as it may not be found due to system size limitations of DFT calculations.

The typical research project focusing on a discovery of a new high-N EM involves the following stages, see Fig. 2.4. At the very beginning, the elemental composition is specified (A, B, C, …), followed by USPEX variable stoichiometry crystal structure search at several pressures covering the interval of experimentally accessible pressures. The goal is to search a large fraction of the full energy landscape and find the global energy minimum structures for each stouchiometry, as well as energetically competitive local minima. Once the structure search at each pressure is completed, the final convex hulls, representing all thermodynamically stable compounds at each pressure, are constructed. Several structures at the vicinity of the convex hull might also be retained to represent possible candidates of metastable compounds. The degree of metastability is defined by the distance from the convex hull for each dynamically stable compound. The dynamical stability is assessed by calculating the phonon spectrum and making sure that there are no imaginary frequency modes

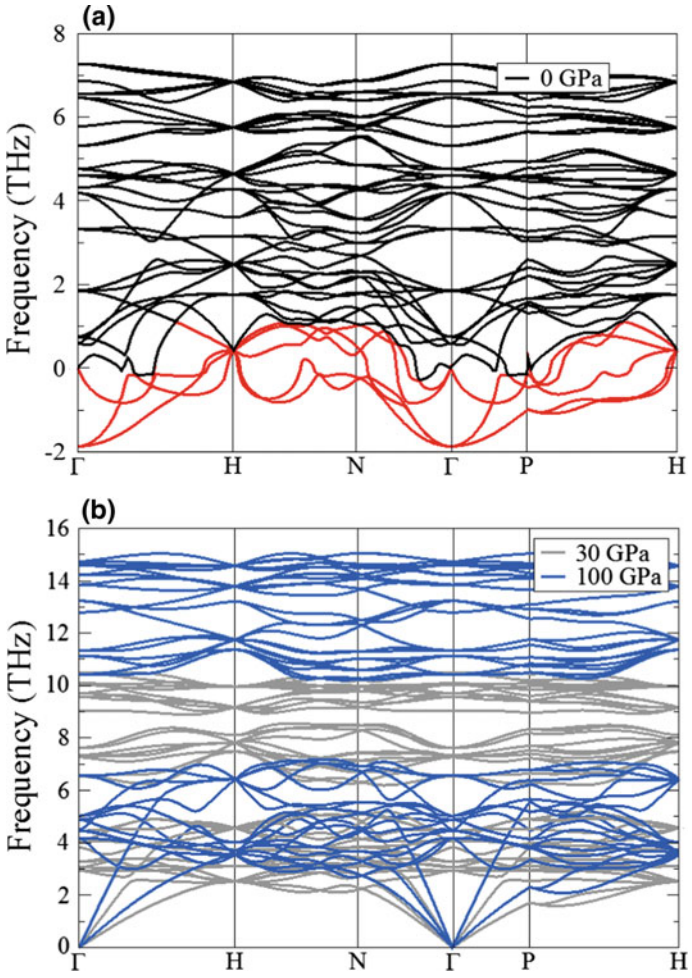

Fig. 2.5 Dynamical stability from phonon spectra: **a** negative/imaginary bands depicted by the red curve signify that this compound is dynamically unstable and is actually a saddle point on the potential energy surface at 0 GPa; **b** phonon spectrum does not have negative/imaginary bands, therefore, this compound is dynamically stable at 50 and 100 GPa

present in the spectrum, see Fig. 2.5. An additional dynamical stability test can be performed by running molecular dynamics simulations at sufficiently-high temperatures and checking whether chemical decomposition of constitutive molecules is observed or not.

Once the stable and metastable compounds are found, their pressure-dependent evolution is investigated to determine the conditions when each of them becomes stable, metastable, or unstable. Then, the possible synthesis routes and mechanisms are explored by identifying specific precursor compounds found during the search

that can be combined in corresponding proportions to produce a specific target compound. To understand whether synthesis can be accomplished by compressing and heating precursors to initiate the high-PT transformations, the evolution of the Gibbs free energy difference between reactants and products is followed as a function of applied pressure to determine whether there is a thermodynamic driving force towards such transformation and at what pressure the target compound becomes energetically preferred in respect to a mixture of the precursor compounds.

The final step of first-principles structure prediction involves calculation of powder X-ray diffraction (XRD) patterns and Raman spectra of the predicted high-N compounds. The XRD patterns (intensity versus 2θ plots) are obtained from known crystal structure by using standard crystallographic XRD software such as POWDER CELL [20] or VESTA [21]. The calculation of Raman spectra is more involved: off-resonant Raman frequencies are obtained within frozen phonon approximation by calculating phonons at the gamma point using DFT, and their intensities are obtained by calculating the derivatives of macroscopic dielectric polarizability tensor along the normal mode eigenvectors.

The crystal structure prediction can only be successful if the results of the search are validated by experimental discovery of the predicted compounds. A combined experimental and theoretical approach involves two interdependent thrusts, see Fig. 2.4. The theory/simulation thrust focuses on searching the energy landscape and eventual prediction of the new stable and metastable compounds. Experimental thrust focuses on high pressure/temperature synthesis of these new compounds by compressing and heating precursors suggested by theory in a diamond anvil cell (DAC) and characterizing the resultant materials using Raman and X-Ray diffraction measurements. The two methods come together by comparing the calculated and experimental XRD patterns and Raman spectra, thus confirming synthesis of new compounds.

2.3 Computational Discovery of High-N Pentazolate Energetic Materials

Although synthesis of cyclo-N_5 pentazolate, an energetic nitrogen oligomer, was attempted since the end of nineteenth century, it was discovered only in the mid-1950s as a part of an aryl pentazole molecule [22, 23] using synthetic organic chemistry methods. This last elusive member of azole series was shown to be aromatic with N–N bond lengths 1.3−1.35 Å, intermediate between single (hydrazine, 1.45 Å) and double (*trans*-diimine, 1.25 Å) bonds [24]. The pentazole (HN_5) or the N_5^- anion [25–30] were not isolated until Vij et al. produced N_5^- in the gas phase in 2002 by cleaving the C–N bond in substituted phenylpentazoles [31, 32]. These pentazolates are important components of high-N energetic materials as they can release a large amount of energy upon conversion of the single-double N–N bonds in the N_5^- aromatic ring to triple N–N bonds in the N_2 molecule. This makes pentazolates

potentially important components for the development of new, green, high-energy-density materials.

Although there exist several metastable nitrogen species, such as linear N_3^- anions [33–35], gas phase pentazolate N_5^- anions [31], N_5^+ chain cations [36], and gas phase N_4 [37], the only other experimentally observed all-nitrogen compounds are covalently bonded non-molecular crystalline phases of nitrogen, which were synthesized at very high pressures (>120 GPa) and temperatures (>2000 K) [4, 5, 15]. We have recently predicted several condensed phase pentazolates [38–40] in an attempt to extend the range of metastability of high-N compounds with the ultimate goal of their recovery at ambient conditions.

Here we review the work directed towards predicting the new pentazolate compounds and suggesting viable transformation pathways of their synthesis from precursor mixtures at high pressures in order to guide experimental synthesis efforts. The idea we pursued in this work is to explore additions to pure nitrogen system, such as alkali metals or hydronitrogens, to achieve enhanced stability and metastability of pentazolates in the solid phase. It was found that the electron-donating species such as alkali metals, ammonium, and hydrogen transfer appreciable negative charge to the N_5 rings, thus enabling both aromaticity in the isolated N_5^- and ionic bonding between non-N cations and pentazolate N_5^- anions within the crystalline environment.

2.3.1 Sodium Pentazolates

Sodium is one of the alkali metals that might be effective in transferring electrons from metallic atoms to nitrogen oligomers. In addition, there is an experimental indication that new high-N compounds containing Na are formed at high pressures and temperatures. In fact, Eremets et al. in 2004 performed experiments by compressing and laser heating sodium azide (NaN_3) precursor to high pressures [35], and observed new peaks in the Raman spectra in the 700–800 cm^{-1} and 1,000–1,300 cm^{-1} range, which can not be attributed to molecular vibrations of the initial azide precursor [41]. They assumed that these new peaks originate from either polymeric nitrogen or a compound containing nitrogen molecular clusters [35]. However, it was impossible to reach an unambiguous conclusion on the nature of the Raman peaks without knowing the structure and composition.

Being motivated by previous experimental attempts, a systematic search of Na_xN_y materials has been attempted using structure prediction method USPEX [38]. The number of atoms in the unit cell in the structure search was varied between 6–16 atoms. To evaluate enthalpies of individuals in USPEX generations, first-principles calculations were performed using the Perdew–Burke–Ernzerhof (PBE) generalized gradient approximation (GGA) functional [42] within density functional theory (DFT) implemented in VASP [43]. The PBE functional was shown to give reliable results for sodium azide [41]. The calculated enthalpies of the predicted structures are used to determine the most stable compounds at a given pressure, thus allowing us

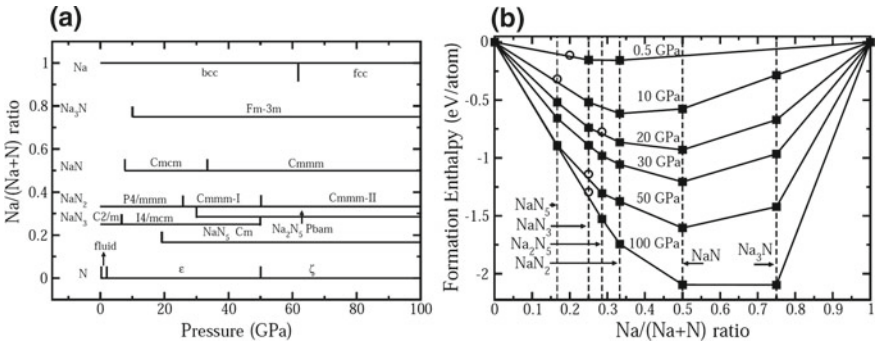

Fig. 2.6 **a** Pressure-composition phase diagram of new Na–N crystal phases discovered in simulations. **b** Convex hull diagram at pressures 0.5, 10, 20, 30, 50, and 100 GPa. Solid squares represent thermodynamically stable phases, open circles—metastable phases. Reprinted with the permission from [38]. Copyright 2016, with permission from Elsevier

to construct the phase diagram of the materials of varying stoichiometry. The crystal structure search methodology is validated by predicting known phases of sodium azide (NaN_3) without any input from experiment. The α-phase of NaN_3 with the symmetry C2/m is found to be the most stable at 0.5 GPa in agreement with experiment, while at 30 GPa the I4/mcm polymorph of NaN_3 appear [44, 45]. At 60 GPa, the P6/m-Na_2N_6 structure containing N_6 rings is found to be the lowest enthalpy phase with a 1:3 sodium to nitrogen ratio.

The convex hull at a range of pressures up to 100 GPa for the Na_xN_y system is given in Fig. 2.6a. The reference structures for the convex hull are α-N_2, ϵ-N_2, and cg-N for nitrogen and bcc-Na and fcc-Na for sodium each taken at corresponding pressure of their stability. Snapshots of several crystal structures found during the search are given in Fig. 2.7.

In order to further justify the adequate accuracy of calculated formation enthalpies using the PBE functional, the convex hull at 50 GPa has been calculated using both PBE functional and the hybrid HSE06 functional [46], see comparison in Fig. 2.8. Overall, both HSE06 and PBE convex hulls are very similar, although the HSE06 formation enthalpies are slightly higher than those calculated using PBE functional, with exception of Na_3N. The HSE06 functional is considered to be state-of-the-art and gives formation enthalpies and atomization energies close to experiment across a wide range of molecules and crystals [47]. Therefore, the similarity of the two curves demonstrates a good accuracy of the PBE calculations of the pentazolate systems reviewed in this chapter.

One interesting result from the structure search was that NaN_3 no longer resides on the convex hull above 50 GPa, thus implying it is thermodynamically unstable beyond this pressure. This results is also reproduced with the HSE06 functional, see Fig. 2.8. Therefore, upon compression in a diamond anvil cell (DAC) above 50 GPa, NaN_3 will transform into a combination of Na_xN_y phases.

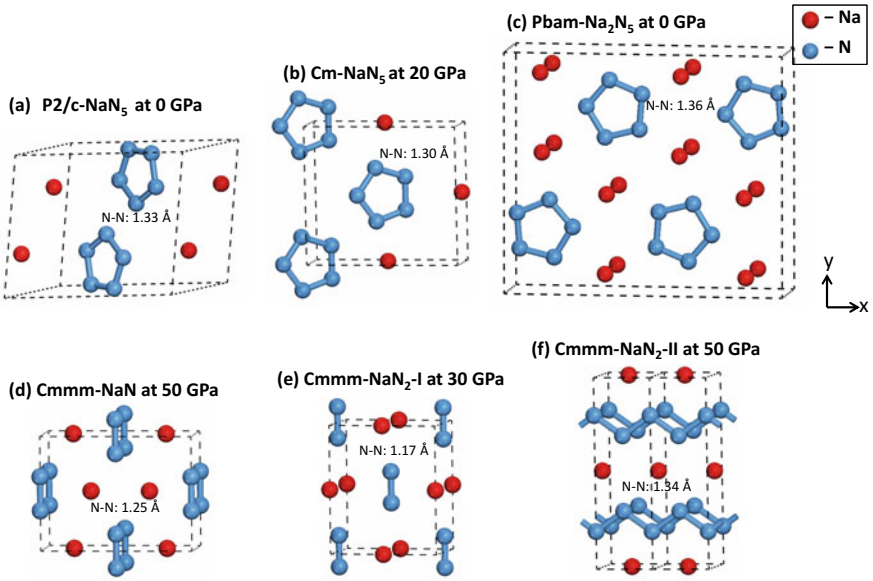

Fig. 2.7 Several newly predicted Na_xN_y crystals at pressures corresponding to where they are thermodynamically stable, or in the case of P2/c-NaN_5 and Pbam-Na_2N_5 metastable at 0 GPa. The space group composition of each structure is shown as well as the N bond length. Reprinted with the permission from [38]. Copyright 2016, with permission from Elsevier

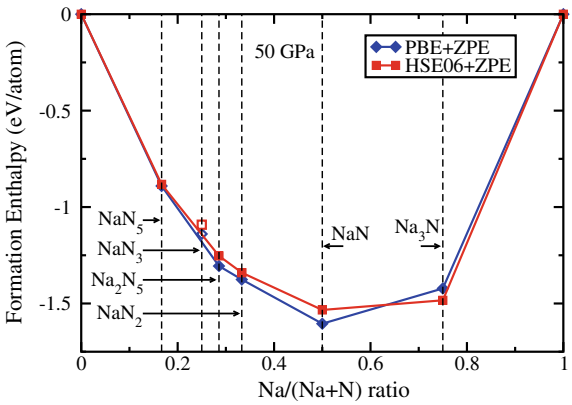

Fig. 2.8 A comparison between the convex hull's calculated with PBE and HSE06 at 50 GPa with zero-point energies (ZPE) included. Reprinted with the permission from [38]. Copyright 2016, with permission from Elsevier

Our search found several high-N crystals containing cyclo-N_5 pentazolate: P2/c-NaN_5, Cm-NaN_5, and Pbam-Na_2N_5, shown in Fig. 2.7a–c. They are found to be on the convex hull from 20 GPa for NaN_5 and 30 GPa for Na_2N_5 up to 100 GPa see Fig. 2.6b. These newly discovered materials can be potential sources of unidentified Raman peaks in experiments on compression of NaN_3 at high pressures [35]. We predict that NaN_5 may be synthesized by compressing NaN_3 above 50 GPa, since NaN_3 becomes unstable above this pressure. Alternatively, direct synthesis of NaN_5

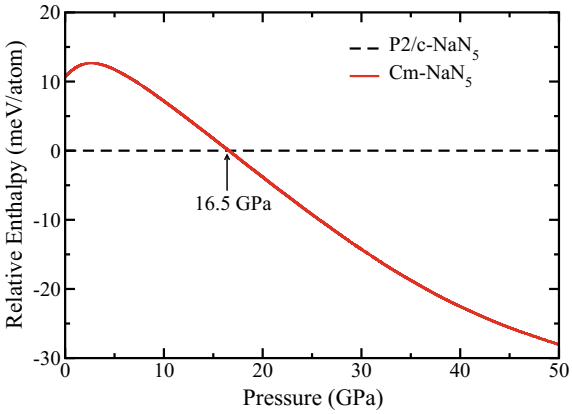

Fig. 2.9 The relative enthalpy of the two phases with NaN_5 stoichiometry. Reprinted with the permission from [38]. Copyright 2016, with permission from Elsevier

can be facilitated by heating and compressing NaN_3 in a DAC using a nitrogen-rich pressure medium via the following chemical reaction, $N_2 + NaN_3 \rightarrow NaN_5$.

To investigate the metastability of new EM materials at ambient conditions, the most energetically preferred polymorphs of NaN_5 and Na_2N_5 are determined by performing fixed composition search at 0 GPa. A new polymorph, P2/c-NaN_5 is found to be the lowest enthalpy structure compared to Cm-NaN_5, see Fig. 2.7a, while Pbam-Na_2N_5, see Fig. 2.7c, remains the only polymorph of Na_2N_5, metastable at ambient conditions as well as at higher pressures. The transition pressure between the high-pressure Cm phase of NaN_5 (Cm-NaN_5) and the zero pressure phase (P2/c-NaN_5) is calculated to be 16.5 GPa, see Fig. 2.9.

To be useful as emergent EMs, the predicted sodium pentazolates must be metastable at ambient conditions. Metastable high-N structures are those that are slightly above the convex hull and dynamically stable, see Sect. 2.2. The dynamical stability of the crystal phases P2/c-NaN_5 and Pbam-Na_2N_5 is determined by checking the absence of any imaginary frequencies in the phonon spectra at 0 GPa in the entire Brillouin zone. Independent check of the dynamical stability of these two phases at 0 GPa is performed by running DFT molecular dynamics simulations at 1,000 K in the NVT ensemble, which displayed no chemical decomposition in the system, thus confirming that both of these phases are dynamically stable at 0 GPa.

To identify the appearance of these newly predicted phases during their synthesis, the Raman and infrared spectroscopy characterization is performed, which includes calculation of the phonon frequencies at the gamma point, followed by the mode assignments. Both structures contain modes in the interval 80–250 cm^{-1} that are lattice modes as well as pentazole librational modes in both phases. Bending modes of the pentazolate molecules have frequencies at 635 cm^{-1} in Pbam-Na_2N_5 and 766 cm^{-1} in P2/c-NaN_5. Deformational modes of the pentazolate molecule have frequencies 900 cm^{-1} in Pbam-Na_2N_5 and 990 cm^{-1} in P2/c-NaN_5. The frequency of the symmetric stretching modes of the pentazolate molecule is at 1,050 cm^{-1} in Pbam-Na_2N_5 and 1,170 cm^{-1} in P2/c-NaN_5.

Table 2.1 Calculated Mulliken charges and Mayer Bond Orders for the nitrogen atoms and bonds in each new crystal at 0 GPa. Reprinted with the permission from [38]. Copyright 2016, with permission from Elsevier

Structure	N-cluster	Charge	Bond order
P2/c-NaN_5	N_5	−0.166	1.42
Pbam-Na_2N_5	N_5	−0.306	1.20
P4/mmm-NaN_2	N_2	−0.340	2.09
Cmmm-NaN_2-II	N-chain	−0.320	1.17
Cmcm-NaN	N_2	−0.630	1.46

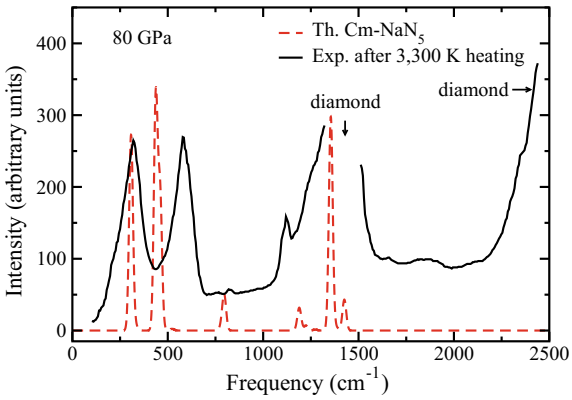

Fig. 2.10 Comparison of theoretical (red dashed line) and experimental (black solid line) [35] Raman spectra of Cm-NaN_5. Reprinted with the permission from [38]. Copyright 2016, with permission from Elsevier

To determine the character of chemical bonding, bond lengths and bond orders are calculated. It was found that the pentazole anions in the NaN_5 and Na_2N_5 crystal phases are aromatic. The N–N bond lengths in the pentazoles are between the N–N single bond (1.449 Å as in hydrazine [48]) and double bond (1.252 Å as in trans-diimine, [49]); see Fig. 2.7a–c. The calculated bond orders are also between the single (1.0) and double (2.0) bond; see Table 2.1. The charge (−0.83 e) and the bond order (1.42) are also close to those found in the gas phase N_5^- anion (−1 e and 1.45 respectively), which displays the structural and chemical similarity of the N_5^- anion in both gas phase and crystalline NaN_5 environments. The calculated band structure demonstrates that P2/c-NaN_5 is an insulator with a band gap of 5 eV while Pbam-Na_2N_5 is metallic.

It is likely that the new sodium pentazolate structures might appear in experiments by Eremets et al. [35]. At pressures above 80 GPa, and a temperature of about 3,000 K, the peaks in the Raman spectrum associated with sodium azide were found to disappear. This is in agreement with the theoretical prediction that sodium azide becomes thermodynamically unstable at high pressures. In addition, the Raman spectrum of the newly predicted sodium pentazolate phase Cm-NaN_5 shows good agreement with that in experiment; see Fig. 2.10. In particular, the agreement is best near 760 cm^{-1} (the pentazole bending mode) and near 1,150 cm^{-1} (the penta-

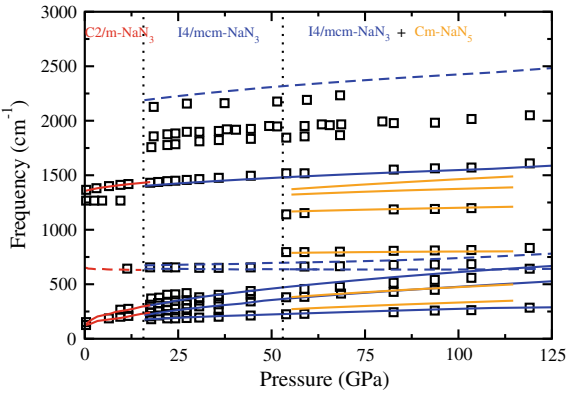

Fig. 2.11 Theoretical NaN_5 and NaN_3 Raman active (solid lines) and IR active (dashed lines) modes as a function of pressure compared to those measured in experiment [35] (black open squares). Reprinted with the permission from [38]. Copyright 2016, with permission from Elsevier

zole deformation mode). Also, in agreement with experiment, the Cm-NaN_5 phase has two lattice modes with appreciable intensity at 307 and 440 cm^{-1} compared to the experimental frequencies at 320 and 580 cm^{-1}. The relatively large difference between the experimental and theoretical frequencies of the second peak may be due the non-hydrostatic effects at 80 GPa which are not considered in our calculations. In addition, it is highly unlikely that NaN_3 will be fully converted into the pure NaN_5 compound. Therefore a one-to-one correspondence between theory and experiment is not expected due to possible appearance of unidentified nitrogen-containing species as well as bulk sodium upon compression and heating of NaN_3.

The theoretical and experimental frequencies of the Raman-active modes of NaN_5 at room temperature as a function of pressure also agree remarkably well, see Fig. 2.11. As shown in Fig. 2.11, the internal Raman-active modes of the pentazole in NaN_5 with frequencies 760 and 1,150 cm^{-1} appear in the experimental spectra above 50 GPa that are not from the initial azide compound. This is in agreement with the prediction that NaN_5 becomes stable above 20 GPa. Since these measurements are performed by compressing NaN_3 at room temperature without additional heating, it expected that complete conversion of NaN_3 into NaN_5 is not achieved. That is why the peaks from sodium azide (NaN_3) are still present in the experimental spectrum up to 100 GPa, see Fig. 2.11. Overall, the agreement between theory and experiment suggests the synthesis of the predicted NaN_5 compound.

2.3.2 Cesium Pentazolates

Although the discovery of NaN_5 consisting of N_5^- was interesting, the experimental evidence for its existence was solely relying on the Raman spectra, which does not directly probe the crystal structure. In order to provide a more definitive conclusion whether alkali pentazolates exist at high pressures, another structure search was performed for cesium polynitrogen compounds at high pressures [39]. The cesium atoms scatter X-rays much more strongly than sodium atoms, therefore it is expected

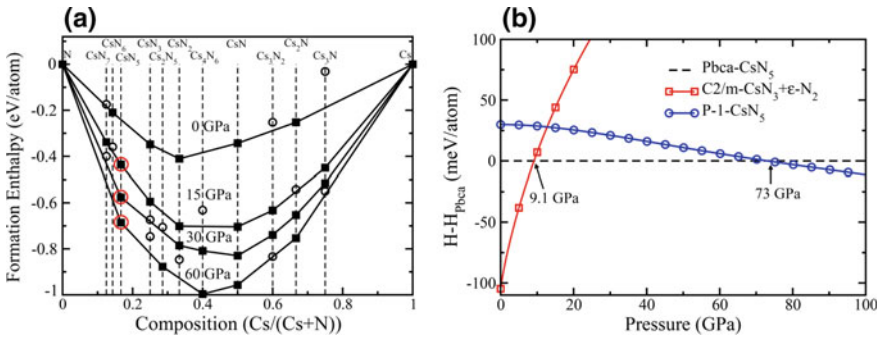

Fig. 2.12 **a** Convex hull diagram at pressures up to 60 GPa. Solid squares represent stable phases, open circles—metastable phases, large red circles—stable CsN_5 phase on the convex hulls. **b** Relative enthalpy difference between two cesium pentazolate (CsN_5) polymorphs and the ε-N_2 phase of solid nitrogen plus the C2/m-CsN_3 phase of cesium azide as a function of pressure. Reprinted with permission from [39]. Copyright (2017) American Chemical Society

that the XRD diffraction pattern would be of much higher quality, thus allowing to unambiguously confirm the experimental synthesis of the new compound.

Therefore, variable composition structure search was performed using the USPEX code for a system consisting of a variable number of cesium and nitrogen atoms (Cs_xN_y) at several pressures up to 60 GPa [39]. The convex hull is first constructed during variable composition search at several pressures, 0, 30, and 60 GPa, followed by fixed stoichiometry crystal structure searches using up to 8 formula units per unit cell. The dispersive correction due to Grimme [50] is added to DFT energy and forces to take into account the long-range van der Waals forces, which are significant in the system under investigation due to the large polarizability of Cs atoms.

The convex hull for the Cs_xN_y system is given in Fig. 2.12a. The reference structures for calculating the formation enthalpy are the α-N_2, ϵ-N_2, and cg-N [4, 7] crystal phases for nitrogen, and the bcc-Cs and Cmca-Cs (Phase V) phases for Cs [51], each taken at its corresponding pressure of stability. The calculations demonstrate that cesium pentazolate salt CsN_5, consisting of pentazolate anion rings (N_5^-) and cesium cations, is on the convex hull at just 15 GPa (Fig. 2.12a). The relative enthalpy difference between the mixture of cesium azide plus dinitrogen ($CsN_3 + N_2$) and reference pentazolate phase Pbca-CsN_5, plotted in Fig. 2.12b, indicates that CsN_5 is energetically preferred above a relatively low pressure of 9.1 GPa. The latter pressure is about 41 GPa lower than the predicted transition pressure of molecular nitrogen to single-bonded threefold coordinated cubic gauche phase of nitrogen (cg-N) in condensed phase [4]. This indicates that the synthesis of CsN_5 requires much lower pressure and temperature stimuli than is needed to synthesize cg-N (over 100 GPa and 2,000 K) [5].

As in case of sodium, discussed in Sect. 2.3.1, CsN_5 consists of isolated N_5 pentazolate anions and Cs cations, see predicted crystal structures in Fig. 2.13. The other compounds discovered during the search are: Cs_2N_5 also consisting of pentazolate molecules; CsN_3 consisting of N_3 azides at pressures from 0–50 GPa and then N_6

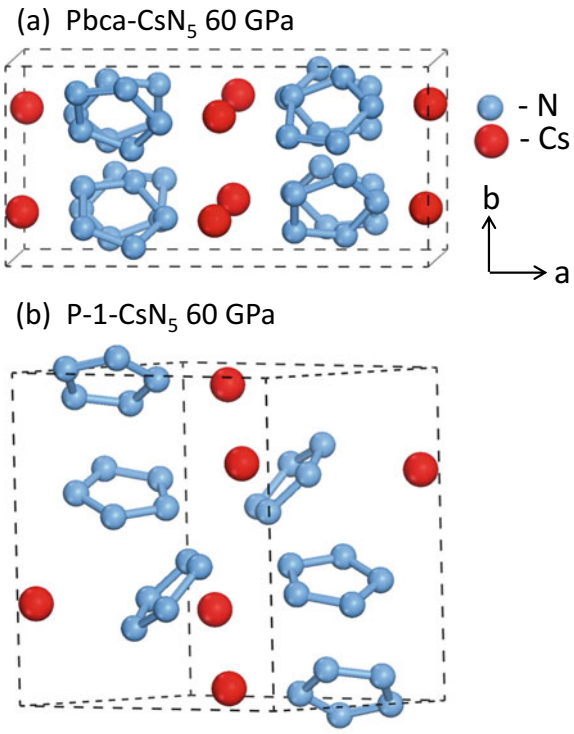

Fig. 2.13 Two energetically competitive cesium pentazolate (CsN_5) polymorphs at 60 GPa discovered during the structure search: **a** Pbca-CsN_5; **b** P-1-CsN_5. Reprinted with permission from [39]. Copyright (2017) American Chemical Society

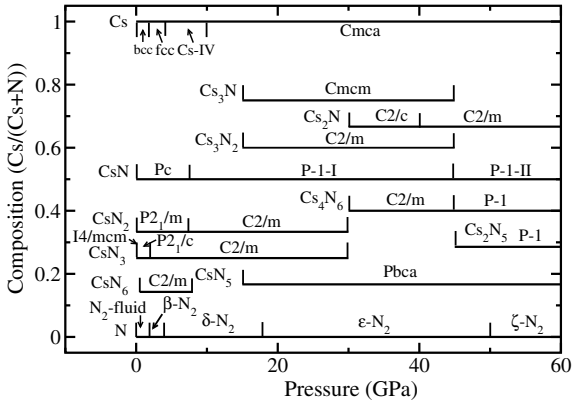

Fig. 2.14 Predicted phase diagram for Cs_xN_y system which contains several novel crystal structures. Reprinted with permission from [39]. Copyright (2017) American Chemical Society

rings at pressures above 50 GPa; CsN_2 consisting of diatomic N_2 anions from 0–40 GPa and then infinite chains of nitrogen above 40 GPa, Cs_4N_6 which consist of N_6 rings from 30 to 60 GPa, CsN which also consist of diatomic N_2 anions from 0–40 GPa and then N_4 chains above 40 GPa; Cs_3N_2 and Cs_2N also containing N_2 anions; and finally Cs_3N consisting of of isolated nitrogen atoms. The summary of the stability pressures for each compound is given in the phase diagram in Fig. 2.14. Note

that although Cs_2N_5 and CsN_3 are not on the hull at 60 GPa, see Fig. 2.12, the R_2N_5 stoichiometry is on the hull for R=Na, and RN_3 is on the hull at lower pressures for both R=Cs and R=Na as shown in Fig. 2.6 [38, 39]. Similar poly-nitrogen compounds have been predicted for other group-I alkali metals [38, 40, 52–54], which implies that nitrogen rings and chains are energetically favorable at high pressures when doped with an alkali metal.

2.3.3 *Pentazole and Ammonium Pentazolate*

Several group-I alkali pentazolates (RN_5) were predicted to be thermodynamically stable at high pressures, but one material that had yet to be found is pentazole HN_5. Hydrogen is unique among group-I elements because it is a gas at ambient conditions and does not become metallic until much higher pressures. In addition, hydrogen can covalently bond to nitrogen to create a rich variety of compounds including ammonia (NH_3), hydrazine (N_2H_4), diimine (N_2H_2), triazene (N_3H_3), tetrazene (N_4H_4), hydrogen azide (N_3H), and ammonium azide (NH_4)(N_3) [55]. The latter compound contains an ammonium cation NH_4^+, which is chemically similar to heavy alkali cations [55–57]. In an analogy with alkali pentazolates, one can also envision the existence of ammonium pentazolate (NH_4)(N_5). Metallic ammonium consisting of NH_4^+ cations glued together by the sea of free electrons has been hypothesized to exist at high pressures inside giant planets such as Uranus and Neptune [56, 57]. It is therefore possible that the high-pressure chemistry of hydronitrogens may be much different than alkali poly-nitrogen compounds.

The high-pressure chemistry of hydronitrogen systems has been recently in the focus of experimental and theoretical investigations [58–64]. The experiments using the mixture of standard precursors, such as molecular N_2 and H_2, with nitrogen content ranging from 5 to 80% suggest the formation of hydronitrogen compounds as evidenced by the disappearance of N_2/H_2 vibrons and the simultaneous appearance of N–H stretching modes [58, 59]. However, a conclusive identification of the type of new nitrogen oligomers or extended networks as well as the determination of the crystal structure have not been made. A hydronitrogen precursor ammonium azide (NH_4)(N_3), containing both H and N, has not shown any signs of chemical transformation upon compression up to 70 GPa [62, 65]. Although theoretical calculations indicate the appearance of polymeric hydronitrogen compounds at a relatively low pressure in a variety of H–N stoichiometries [60, 63, 64], no such transformation was observed in experiment when hydrogen azide is compressed to high pressures [66].

To bridge the bap between experiment and theory, novel hydronitrogen crystalline compounds have been searched at high pressure using first-principle crystal structure prediction [40]. The goal is to understand whether pentazolate compounds such as pentazole N_5H and ammonium pentazolate (NH_4)(N_5) do exist and to identify specific conditions needed for their synthesis. Variable composition USPEX calculations are performed at 30 and 60 GPa. After the variable composition search is completed, fixed-compositions structure searches with larger number of atoms

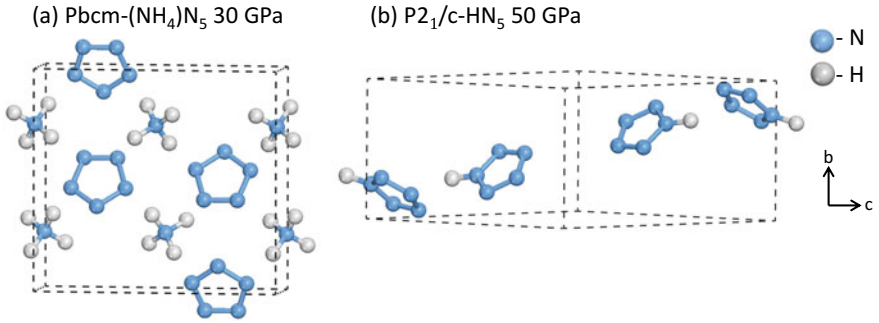

Fig. 2.15 New hydronitrogen pentazolate compounds discovered during N_xH structure search: **a** ammonium pentazolate $(NH_4)(N_5)$, and **b** pentazole N_5H. Reprinted with permission from [40]. Copyright (2017) American Chemical Society

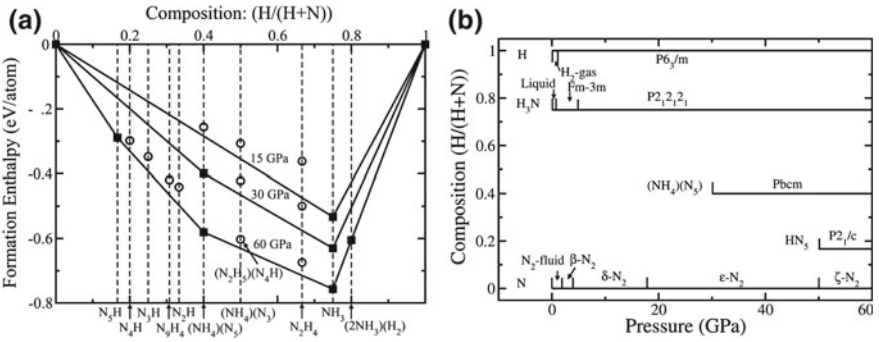

Fig. 2.16 Hydronitrogen phase diagram: **a** formation enthalpy-composition convex hull, and **b** the crystal structure/pressure stability diagram. At 15 and 30 GPa the elemental N structure is ε-N_2 and at 60 GPa—cg-N. For all pressures the elemental hydrogen crystal structure has space group $P6_3/m$ [67]. Reprinted with permission from [40]. Copyright (2017) American Chemical Society

(up to 40 atoms/unit cell) are performed to find the lowest enthalpy structure for each composition.

Two new crystalline materials, ammonium pentazolate $(NH_4)(N_5)$, and pentazole N_5H, are found, featuring all-nitrogen cyclic pentazoles, see Fig. 2.15a, b. The first crystal, $(NH_4)(N_5)$, containing isolated ammonium cations NH_4^+ and pentazolate anions N_5^- (Fig. 2.15a), appears on the convex hull at 30 GPa (Fig. 2.16). The second crystal, N_5H, consists of cyclo-N_5 covalently bonded to a H atom (Fig. 2.15b), and appears on the convex hull at 50 GPa. Both structures are predicted to be dynamically stable at 50 GPa for N_5H and 30 GPa for $(NH_4)(N_5)$ as they lack any imaginary frequencies in the phonon spectrum in the entire Brillioun zone.

The appearance of these two new compounds dramatically modifies the convex hulls at lower pressures. In particular, the only thermodynamically stable crystals at 60 GPa are pentazole N_5H, ammonium pentazolate $(NH_4)(N_5)$, ammonia NH_3, and a crystal containing a mixture of NH_3 and H_2 molecules with net stoichiometry NH_4

(Fig. 2.16a). The formation enthalpy of hydrazine N_2H_4 [68] is also calculated to be above the convex hull, therefore it is also metastable. At a lower pressure of 30 GPa, ammonium pentazolate $(NH_4)(N_5)$ is still thermodynamically stable, whereas pentazole N_5H is not. At 15 GPa, $(NH_4)(N_5)$ is marginally metastable, leaving only one stable compound—ammonia (NH_3) (Fig. 2.16a). Another known metastable compound, ammonium azide $(NH_4)(N_3)$ with symmetry P2/c [69] (and stoichiometry N_4H_4) is also displayed at 15 and 30 GPa. Ammonium azide is predicted to undergo the phase transition to trans-tetrazene (TTZ) at 42 GPa [62], followed by another transition at higher pressure to a crystal that consists of N_2H_5 molecules and infinite nitrogen chains (N_4H) [64] therefore, the lowest enthalpy polymorph of metastable (N_4H_4) with P1 space group is shown at 60 GPa as well.

Both pentazole and ammonium pentazolate crystals contain aromatic cyclo-N_5 with the N–N bond lengths 1.30–1.35 Å, which are intermediate between single N–N (1.45 Å) and double N=N (1.25 Å) bonds. The strength of the aromatic N–N bond in the N_5^- ring in the predicted crystals $P2_1/c$-N_5H and Pbcm-$(NH_4)(N_5)$ is approximately the same as that in the gas phase. To quantify this conclusion, the total Mulliken charges, Mayer bond orders, and bond lengths in the N_5^- ring in both the crystalline environment and the gas phase are calculated at 0 GPa and reported in Fig. 2.17. In the case of N_5H this comparison is straightforward as the structural unit

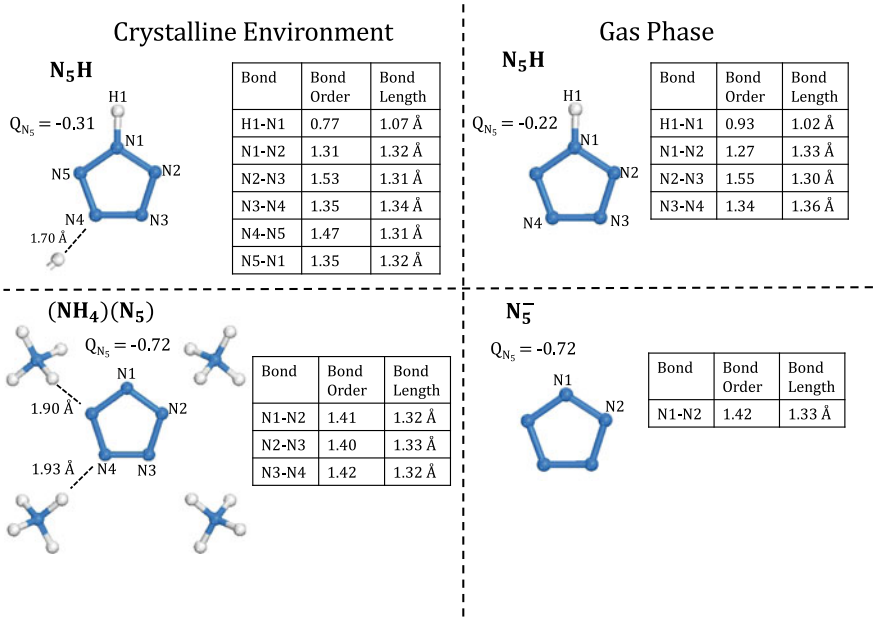

Fig. 2.17 Total Mulliken charges, Mayer bond orders, and bond lengths in the N_5^- ring in $P2_1/c$-N_5H and Pbcm-$(NH_4)(N_5)$ crystals compared to those in gas phase N_5H and N_5. The N···H, hydrogen bonds are also shown in both crystalline environments. Reprinted with permission from [40]. Copyright (2017) American Chemical Society

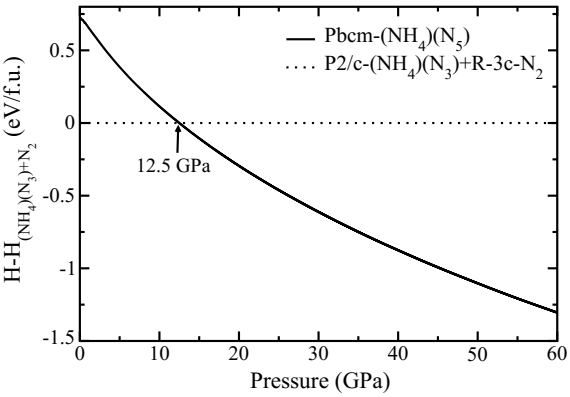

Fig. 2.18 The enthalpy difference between the predicted ammonium pentazolate ($Pbcm$-$(NH_4)(N_5)$) crystal and ammonium azide ($P2/c$-$(NH_4)(N_3)$) plus dinitrogen (R–3c–N_2). The predicted transition pressure is 12.5 GPa. Reprinted with permission from [40]. Copyright (2017) American Chemical Society

N_5H is electrically neutral. The N_5 bond lengths and bond orders are mostly the same in both the gas phase and in the crystalline environments, except for bonds N4–N5 and N5–N1 which have a larger bond order compared to the gas phase, see Fig. 2.17. The bond lengths of both crystalline and gas phase N_5H are in a good agreement with those calculated by Ferris and Bartlett [25].

To make a unique comparison of bond orders of the N_5 ring in crystalline $(NH_4)(N_5)$ with those in the gas phase N_5, its negative charge (-0.72 e) was fixed to that in the crystalline $(NH_4)(N_5)$. The bond lengths ($\approx$1.33 Å) and bond orders ($\approx$1.42) in both environments are very close, the gas phase N_5^- possesses fivefold D_{5h} symmetry so each bond length and bond order are the same.

Ammonium pentazolate was predicted to become thermodynamically stable at lower pressure (30 GPa) than pentazole N_5H (50 GPa). To achieve its synthesis, the stoichiometrically balanced mixture of ammonium azide $(NH_4)(N_3)$ and diatomic nitrogen (N_2) should be compressed to high pressures in a diamond anvil cell to activate the chemical reaction $(NH_4)(N_3) + N_2 \rightarrow (NH_4)(N_5)$. The pressure-dependent enthalpy difference between the products and reactants for this transformation shown in Fig. 2.18 displays the possibility of the phase transformation at relatively low pressure of 12.5 GPa. Ammonium azide alone has been reported to be chemically stable upon compression up to 70 GPa at room temperature [62]. However, setting up the right stoichiometry in the diamond anvil cell by adding N_2 might activate the conversion of the azide (N_3^-) anions and N_2 molecules to the N_5^- ring at pressures above 12.5 GPa. The higher pressures and temperatures seem to be required to overcome the significant energy barrier associated with this transformation.

2.4 Comparison of Pentazolate Crystals

The predicted crystal structures, phase transition pressures, and pressure range of stability of crystal phase pentazolates RN_5 are summarized in Table 2.2. Their crystals structures are different: all but a couple possess a different space group

Table 2.2 Comparison of various pentazolates RN_5: the predicted crystallographic space groups, phase transition pressures, range of stability, charges and bond orders

Stoichiometry	Space groups	Pressure range of stability (GPa)	N_5 Charge	N_5 bond order
HN_5	$P2_1/c$ [40]	50–70	−0.31	1.31
$(NH_4)N_5$	Pbcm [40]	30–60	−0.72	1.41
LiN_5	$P2_1/c$ 65 GPa → C2/c [54]	15–100	–	–
	$P2_1$ 20 GPa → $P2_1/m$ [52]	10–100	–	1.42
NaN_5	Cm: 20–100 GPa [38]	20–100	−0.83	1.42
CsN_5	Pbca 73 GPa → P-1 [39]	15–100	−0.85	1.41
	$Cmc2_1$ [53]	14–100	−0.85	1.37–1.46

symmetry. Although LiN_5 and HN_5 crystals have the same space group symmetry $P2_1/c$, molecular constituents are different: N_5^- in LiN_5 and HN_5 in HN_5 crystal. One possible reason for the diversity of crystal structures is that the steric repulsion between cations of different alkali atoms varies greatly when moving down the column of the periodic table. Therefore, as the atomic radius gets larger, the packing and orientation of the N_5 molecules may change resulting in different crystal volumes and different molecular arrangements within the unit cell, especially at high pressures when the PV term in the enthalpy becomes significant.

The charge transfer from cations to N_5^- ring anions enhances the stability of crystal phase pentazolates as it enables aromaticity and increases the electrostatic attraction between ions. The calculated charges and bond orders in the N_5 ring are almost identical among different pentazolate salts, see Table 2.2. The main exception is pentazole (HN_5) which has a smaller amount of negative charge on the N_5 ring, see Table 2.2. An interesting observation is that there is an inverse relationship between the amount of charge transfer to N_5 ring and the stability pressure of pentazolate crystals, see Table 2.2. HN_5 has the smallest charge transfer which causes the pressure of stability to increase up to 50 GPa, while $(NH_4)N_5$ only has slightly less charge transfer than the alkali pentazolates so the pressure of stability is reduced to 30 GPa. In contrast, the pressure of stability decreases down to 10–20 GPa for alkali-metal pentazolates which also have the largest charge transfer to N_5, see Table 2.2. The small charge transfer to N_5 in HN_5 also lowers the bond order slightly in comparison to alkali pentazolates as shown in Table 2.2, which might also play a role in increasing the stability pressure.

All the alkali pentazolates reviewed in this paper have been predicted to be metastable at ambient conditions with no imaginary frequencies and no decomposition observed at high temperature MD simulations [38, 52]. However, pentazole (HN_5) and ammonium pentazolate $(NH_4)N_5$ are not dynamically stable at ambient conditions [40], which seems to be due to reduced charge transfer to N_5.

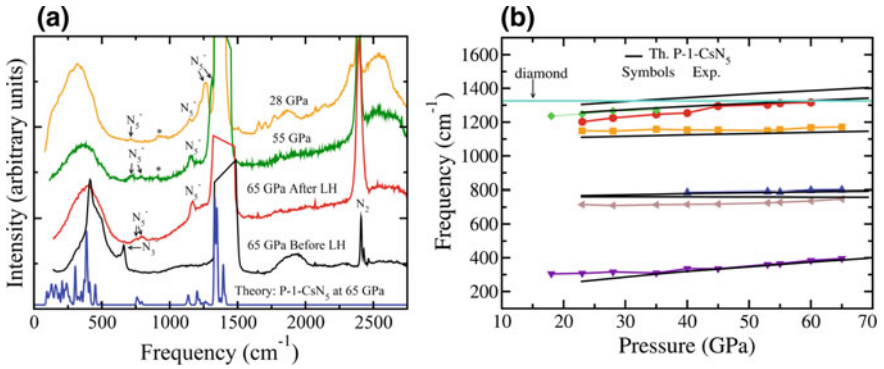

Fig. 2.19 **a** Experimental Raman spectra of the $CsN_3 + N_2$ mixture at 65 GPa before laser heating (LH) (black curve), and of CsN_5 after LH (red curve) then upon decompression to 55 GPa (green curve) and 28 GPa (amber curve). Theoretical Raman spectrum of P-1-CsN_5 polymorph (blue curve) is also shown for comparison. Arrows indicate N_5^- peaks. **b** Pressure dependence of experimental and theoretical frequencies of Raman-active modes of CsN_5: theory—black lines, experiment—colored symbols connected by different colored lines for different modes. The light blue line represents the lower frequency of the first-order Raman scattering of diamond. Reprinted with permission from [39]. Copyright (2017) American Chemical Society

2.5 Synthesis of Cesium Pentazolate (CsN_5)

Theoretical prediction of CsN_5 and its enhanced stability at relatively low pressures stimulated the experimental effort to synthesize this material. It was predicted that compressing cesium azide in a nitrogen-rich environment might cause simple reaction $CsN_3 + N_2 \rightarrow CsN_5$ which is calculated to be energetically favorable above a pressure of just 9.1 GPa, see Fig. 2.12 [39]. Therefore, experiment was set up to compress CsN_3 in a diamond anvil cell (DAC) filled cryogenically with nitrogen N_2, the latter serving both as a pressure transmitting medium and reagent.

It was observed during the experiment that laser heating (LH) of CsN_3 and N_2 mixture at 65 GPa results in disappearance of the azide modes and appearance of the N_5 pentazolate modes in the Raman spectra, see Fig. 2.19a. The azide ν_1 mode is a shoulder of the diamond first-order peak at 1,490 cm^{-1} at 65 GPa, which disappears after LH. The N_5^- breathing mode is also very close to the diamond peak but is visible in the spectrum at 55 GPa at frequency 1,320 cm^{-1}. The other two modes associated with the azide anion N_3^- also disappear: sharp peaks ν_2 at 656 cm^{-1} and the broad peak in the 1,750–2,000 cm^{-1} frequency range see Fig. 2.19a. New Raman peaks also appear between 700 and 850 cm^{-1}, and at 1,170 and 1,320 cm^{-1} associated with N_5. Both the relative intensities and the frequencies of the experimentally observed Raman peaks are in agreement with those of the theoretically predicted Raman modes of P-1-CsN_5, see Fig. 2.19a. The observed Raman modes at 55 GPa were assigned as follows: 1,320 cm^{-1} – N_5^- ring breathing; 1,170 cm^{-1} – N_5^- antisymmetric N–N breathing and angle deformations, and 700–850 cm^{-1} – N_5^- ring bending and

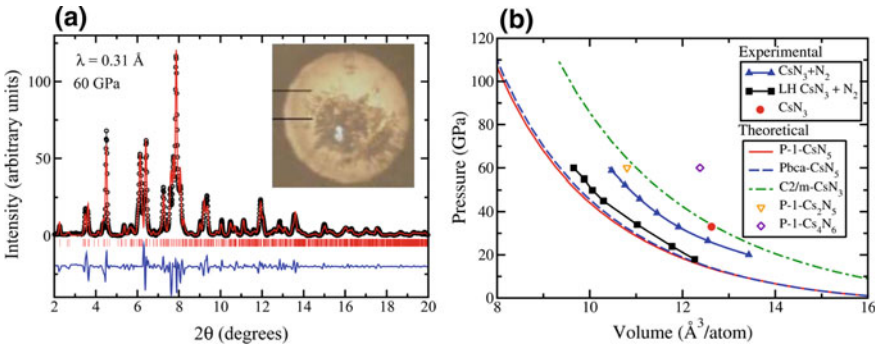

Fig. 2.20 **a** Measured X-Ray diffraction patterns (black circles) after laser heating against the Le Bail fit (red solid line) using predicted crystal structure of P-1-CsN_5. Vertical red ticks mark positions of Bragg peaks. The blue line is the difference between the measured and fitted intensities. The inset shows a microphotograph of the sample after heating in transmitted light, indicating the transparency of the synthesized phase. **b** Comparison of the measured and calculated pressure versus volume equation of state (EOS) for the synthesized compound: experimental data are plotted with solid symbols, whereas theoretical predictions—by open symbols and lines. Also shown are the experimental (P, V) points corresponding to CsN_3 at 33 GPa and the EOS of $CsN_3 + N_2$ mixture before laser heating (LH). Reprinted with permission from [39]. Copyright (2017) American Chemical Society

librational modes. Upon pressure release, the intensity of the Raman modes of CsN_5 dropped substantially, and only the most intense internal N_5 mode (1,236 cm^{-1}) and the intense broad feature at the low frequency interval (0–550 cm^{-1}) were observed below 20 GPa, see Fig. 2.19b. Upon further release of pressure below 18 GPa, all Raman modes other than the one corresponding to high frequency nitrogen vibrons disappear. The N_2 vibrons were always present because nitrogen was the pressure transmitting medium.

Additional confirmation of CsN_5 synthesis comes from XRD measurements during the compression experiments which reveal the appearance of new intense and narrow Bragg peaks with a simultaneous disappearance of the broad CsN_3 peaks. The Bragg peaks of the new phase are well indexed using the theoretically predicted P-1-CsN_5 structure. The resultant Le Bail-fitted and experimental XRD patterns at 60 GPa, shown in Fig. 2.20a, are well-matched. The lattice parameters obtained from the Le Bail refinement are close to those predicted by theory. The comparison between the experimental pressure versus volume equation of state (EOS) with the theoretical EOS of CsN_5 and various candidate structures obtained during the evolutionary structure search is shown in Fig. 2.20b. The experimental EOS matches the theoretical EOSs well for both P-1-CsN_5 and Pbca-CsN_5 phases in the full range of applied pressures. In addition, the experimental volume of $CsN_3 + N_2$ after laser heating is 10% less than the sum of volumes of CsN_3 and N_2 before laser heating at a given pressure. This provides a strong indication of major atomic rearrangements to form N_5 rings during the conversion of $CsN_3 + N_2$ to CsN_5.

2.6 Conclusions

This review of a novel family of poly-nitrogen compounds demonstrates the power of first-principles crystal structure search methods for the discovery of new materials. The novelty of this work is in framing the theoretical effort as an integral part of joint experimental and theoretical exploration of materials chemistry. Theory/simulation guidance not only involves the prediction of chemical composition and crystal structure of new compounds, but it also suggests specific precursors, and experimental conditions for experimental synthesis of high-N pentazolate EMs. The ultimate success was achieved in joint theoretical and experimental discovery of cesium pentazolate, which was synthesized by compressing and heating cesium azide CsN_3 and N_2 precursors in diamond anvil cell.

This success story paves the way for synthesis of novel high-N energetic materials with the promise of quenching their metastable phases at ambient conditions. In fact, the theoretical work on prediction of new pentazolate compounds inspired a renewed attempt to synthesize of cyclo-N_5^- compounds using traditional methods of organic synthesis [70–73]. A breakthrough has been achieved very recently in synthesis of N_5^- compounds by three independent groups both at ambient pressure and at high pressures [39, 70–73]. The ambient pressure synthesis involved the cleavage of the C–N bond in arylpentazoles [72] followed by stabilizing the N_5^- anion with various cations such as hydronium, ammonium, sodium, chloride, cobalt, iron, or manganese [70–72, 74]. The computational discovery of alkali and hydronitrogen pentazolates demonstrates the diversity of metastable high-N compounds, thus opening up new routes for their synthesis and recovery at ambient conditions.

References

1. Klapötke TM (2015) Chemistry of high-energy materials. De Gruyter, Berlin, München, Boston
2. Nobel A (1868) Improved explosive compound. US Patent 78,317
3. Christe K (2007) Propellants Explos Pyrotech 32(3):194
4. Mailhiot C, Yang L, McMahan A (1992) Phys Rev B 46(22):14419
5. Eremets MI, Gavriliuk AG, Trojan IA, Dzivenko DA, Boehler R (2004) Nat Mat 3(8):558
6. Eremets MI, Gavriliuk AG, Trojan IA (2007) Appl Phys Lett 90(17):171904
7. Gregoryanz E, Goncharov AF, Sanloup C, Somayazulu M, Mao Hk, Hemley RJ (2007) J Chem Phys 126(18):184505
8. Lipp M, Klepeis J, Baer B, Cynn H, Evans W, Iota V, Yoo CS (2007) Phys Rev B 76(1):014113
9. Maddox J (1988) Nature 335(6187):201
10. Oganov AR, Glass CW (2006) J Chem Phys 124(24):244704
11. Pickard CJ, Needs RJ (2011) J Phys Cond Matt 23(5):053201
12. Zhu Q, Oganov AR, Zhou XF (2014) Top Curr Chem 345:223
13. Wang Y, Lv J, Zhu L, Ma Y (2012) Comput Phys Commun 183(10):2063
14. Ma Y, Oganov A, Li Z, Xie Y, Kotakoski J (2009) Phys Rev Lett 102(6):100
15. Tomasino D, Kim M, Smith J, Yoo CS (2014) Phys Rev Lett 113:205502
16. Zhang W, Oganov AR, Goncharov AF, Zhu Q, Boulfelfel SE, Lyakhov AO, Stavrou E, Somayazulu M, Prakapenka VB, Konôpková Z (2013) Science 342(6165):1502

17. Duan D, Liu Y, Tian F, Li D, Huang X, Zhao Z, Yu H, Liu B, Tian W, Cui T (2014) Sci Rep 4:6968
18. Drozdov AP, Eremets MI, Troyan IA, Ksenofontov V, Shylin SI (2015) Nature 525(7567):73
19. Oganov AR, Chen J, Gatti C, Ma Y, Ma Y, Glass CW, Liu Z, Yu T, Kurakevych OO, Solozhenko VL (2009) Nature 457
20. Kraus W, Nolze G (1996) J Appl Crystallogr 29(3):301
21. Momma K, Izumi F (2011) J Appl Crystallogr 44(6):1272
22. Huisgen R, Ugi I (1957) Chem Ber 90(12):2914
23. Clusius K, Hurzeler H (1954) Helvetica Chimica Acta 37(3):798
24. Wallis JD, Dunitz JD (1983) J Chem Soc Chem Commun (16):910
25. Ferris KF, Bartlett RJ (1992) J Am Chem Soc 114(21):8302
26. Butler RN (1996) In: Katritzky AR, Rees CW, Scriven EF (eds) Comprehensive heterocyclic chemistry II. Elsevier, New York, pp 897–904
27. Ugi I (1984) In: Katritzky AR, Ree (eds) Comprehensive heterocyclic chemistry I. Elsevier, New York, pp 839–845
28. Burke LA, Butler RN, Stephens JC (2001) J Chem Soc Perkin Trans 2(9):1679
29. Janoschek R (1993) Angew Chem Int Ed 32(2):230
30. Nguyen MT, Ha TK (2001) Chem Phys Lett 335:311
31. Vij A, Pavlovich JG, Wilson WW, Vij V, Christe KO (2002) Angew Chem 141(16):3177
32. Östmark H, Wallin S, Brinck T, Carlqvist P, Claridge R, Hedlund E, Yudina L (2003) Chem Phys Lett 379(5–6):539
33. Evans BL, Yoffe AD, Gray P (1959) Chem Rev 59(4):515
34. Peiris SM, Russell TP (2003) J Phys Chem A 107:944
35. Eremets MI, Popov MY, Trojan IA, Denisov VN, Boehler R, Hemley RJ (2004) J Chem Phys 120(22):10618
36. Christe KO, Wilson WW, Sheehy JA, Boatz JA (1999) Angew Chem Int Ed 40(16):2947
37. Cacace F, de Petris G, Troiani A (2002) Science 295:480
38. Steele BA, Oleynik II (2016) Chem Phys Lett 643:21
39. Steele BA, Stavrou E, Crowhurst JC, Zaug JM, Prakapenka VB, Oleynik II (2017) Chem Mater 29(2):735
40. Steele BA, Oleynik II (2017) J Phys Chem A 121:1808
41. Steele BA, Landerville AC, Oleynik II (2014) J Phys Conf Ser 500(16):162005
42. Perdew J, Burke K, Ernzerhof M (1996) Phys Rev Lett 77(18):3865
43. Kresse G, Furthmiiller J (1996) Comput Mat Sci 6(1):15
44. Zhang M, Yin K, Zhang X, Wang H, Li Q, Wu Z (2013) Solid State Commun 161:13
45. Millar DIA, Barry C, Marshall WG, Pulham CR (2014) Z Kristallogr 229(3):259
46. Heyd J, Scuseria GE, Ernzerhof M (2003) J Chem Phys 118(18):8207
47. Schimka L, Harl J, Kresse G (2011) J Chem Phys 134(2):024116
48. Morino Y, Ijima T, Murata Y (1960) Bull Chem Soc Jpn 33(1):46
49. Carlotti M, Johns JWC, Trombetti A (1974) Can J Phys 52(4):340
50. Grimme S (2006) J Comput Chem 27(15):1787
51. Takemura K, Christensen N, Novikov D, Syassen K, Schwarz U, Hanfland M (2000) Phys Rev B 61(21):14399
52. Peng F, Yao Y, Liu H, Ma Y (2015) J Phys Chem Lett 6(12):2363
53. Peng F, Han Y, Liu H, Yao Y (2015) Sci Rep 5:16902
54. Shen Y, Oganov AR, Qian G, Zhang J, Dong H, Zhu Q, Zhou Z (2015) Sci Rep 5:14204
55. Wiberg E (2001) Inorganic chemistry. Academic Press
56. Stevenson DJ (1975) Nature 258(5532):222
57. Bernal MFM, Massey HSW (1954) Mon Not Roy Astron Soc 114(2):172
58. Goncharov AF, Holtgrewe N, Qian G, Hu C, Oganov AR, Somayazulu M, Stavrou E, Pickard CJ, Berlie A, Yen F, Mahmood M, Lobanov SS, Konôpková Z, Prakapenka VB (2015) J Chem Phys 142(21):214308
59. Wang H, Eremets MI, Troyan I, Liu H, Ma Y, Vereecken L (2015) Sci Rep 5:13239
60. Yin K, Wang Y, Liu H, Peng F, Zhang L (2015) J Mater Chem A 3(8):4188

61. Spaulding DK, Weck G, Loubeyre P, Datchi F, Dumas P, Hanfland M (2014) Nat Commun 5:5739
62. Crowhurst JC, Zaug JM, Radousky HB, Steele BA, Landerville AC, Oleynik II (2014) J Phys Chem A 118(38):8695
63. Hu A, Zhang F (2011) J Phys Cond Matt 23(2):022203
64. Qian GR, Niu H, Hu CH, Oganov AR, Zeng Q, Zhou HY (2016) Sci Rep 6:25947
65. Medvedev S, Eremets M, Evers J, Klapotke T, Palasyuk T, Trojan I (2011) Chem Phys 386(1–3):41
66. Evers J, Gobel M, Krumm B, Martin F, Medvedyev S, Oehlinger G, Steemann FX, Troyan I, Klap TM, Eremets MI (2011) J Am Chem Soc 133:12100
67. Pickard CJ, Needs RJ (2007) Nat Phys 3(7):473
68. Chellappa R, Dattelbaum D, Daemen L, Liu Z (2014) J Phys Conf Ser 500:052008
69. Yu H, Duan D, Tian F, Liu H, Li D, Huang X, Liu Y, Liu B, Cui T (2015) J Phys Chem C 119(45):25268
70. Bazanov B, Geiger U, Carmieli R, Grinstein D, Welner S, Haas Y (2016) Ang Chem 1–4
71. Xu Y, Wang Q, Shen C, Lin Q, Wang P, Lu M (2017) Nature 549(7670):78
72. Zhang C, Sun C, Hu B, Yu C, Lu M (2017) Science 355(6323)
73. Zhang C, Yang C, Hu B, Yu C, Zheng Z, Sun C (2017) Angew Chem Int Ed 56(16):4512
74. Zhang C, Sun C, Hu B, Lu M (2017) Science 355:374